

AD-A090 561

SOUTHWEST RESEARCH INST SAN ANTONIO TEX F/6 11/6  
FATIGUE MICROCRACK BEHAVIOR UNDER THE INFLUENCE OF SURFACE RESI--ETC(U)  
OCT 80 J E HACK, G R LEVERANT N00014-78-C-0674

NK

UNCLASSIFIED

1 of 1  
AD-  
ADHESAT

END  
DATE  
FILMED  
11 80  
DTIC

**LEVEL**  
1075285

(12)

AD A090561

# FATIGUE MICROCRACK BEHAVIOR UNDER THE INFLUENCE OF SURFACE RESIDUAL STRESSES

J. E. Hack and G. R. Leverant  
Southwest Research Institute  
P.O. Drawer 28510  
San Antonio, Texas 78284

DTIC  
ELECT  
OCT 9 1980  
C

**INTERIM REPORT for Period August 1, 1979 - July 31, 1980**  
**Contract N00014-78-C-0674**

Reproduction in whole or in part is permitted for any purpose of the United States Government. Distribution is unlimited.

Prepared for  
**OFFICE OF NAVAL RESEARCH**  
800 North Quincy Street  
Arlington, Virginia  
22217

DISTRIBUTION STATEMENT A  
Approved for public release;  
Distribution Unlimited

October 1, 1980

NR 031-812

DDC FILE COPY



**SOUTHWEST RESEARCH INSTITUTE**  
SAN ANTONIO HOUSTON

UNCLASSIFIED

SECURITY CLASSIFICATION OF THIS PAGE (When Data Entered)

REPORT DOCUMENTATION PAGE		READ INSTRUCTIONS BEFORE COMPLETING FORM
1. REPORT NUMBER	2. GOVT ACCESSION NO. <b>AD-A090</b>	3. RECIPIENT'S CATALOG NUMBER <b>561</b>
4. TITLE (and Subtitle) <b>FATIGUE MICROCRACK BEHAVIOR UNDER THE INFLUENCE OF SURFACE RESIDUAL STRESSES</b>		5. TYPE OF REPORT & PERIOD COVERED <b>Interim Report August 1, 1979-July 31, 1980</b>
7. AUTHOR(s) <b>J. E. Hack G. R. Leverant</b>		6. PERFORMING ORG. REPORT NUMBER <b>02-5382</b>
9. PERFORMING ORGANIZATION NAME AND ADDRESS <b>Southwest Research Institute P. O. Drawer 28510 San Antonio, Texas 78284</b>		8. CONTRACT OR GRANT NUMBER(s) <b>NO0014-78-C-0674</b>
11. CONTROLLING OFFICE NAME AND ADDRESS <b>Office of Naval Research 800 North Quincy Street Arlington, Virginia 22217</b>		10. PROGRAM ELEMENT, PROJECT, TASK AREA & WORK UNIT NUMBERS <b>Project Element 122201 NR031-812/6-23-78(471)</b>
14. MONITORING AGENCY NAME & ADDRESS (if different from Controlling Office) <b>1246</b>		12. REPORT DATE <b>October 1, 1980</b>
		13. NUMBER OF PAGES <b>39 + prelims</b>
		15. SECURITY CLASS. (of this report) <b>UNCLASSIFIED</b>
		15a. DECLASSIFICATION DOWNGRADING SCHEDULE
16. DISTRIBUTION STATEMENT (of this Report) <b>Reproduction in whole or in part is permitted for any purpose of the United States Government. Distribution is unlimited.</b>		
17. DISTRIBUTION STATEMENT (of the abstract entered in Block 20, if different from Report)		
18. SUPPLEMENTARY NOTES		
19. KEY WORDS (Continue on reverse side if necessary and identify by block number) <b>Fatigue                      Titanium Microcrack                  Surface Crack Opening Displacement Residual Stress              Stress Intensity</b>		
20. ABSTRACT (Continue on reverse side if necessary and identify by block number) <b>-&gt;Direct observations of the surface crack opening displacement (SCOD) of surface and corner cracks were made on samples of Ti-6Al-4V under both cyclic and static loading conditions. The observations were conducted in a specially designed loading stage <u>in-situ</u> in a scanning electron microscope. Cracks from 7-1300µ have been studied by this technique. Results show that surface residual stresses can significantly affect crack opening behavior, thus crack growth behavior, even when the crack has grown well beyond the</b>		

DD FORM 1473

1 JAN 73

EDITION OF 1 NOV 65 IS OBSOLETE

UNCLASSIFIED

SECURITY CLASSIFICATION OF THIS PAGE (When Data Entered)

UNCLASSIFIED

SECURITY CLASSIFICATION OF THIS PAGE(When Data Entered)

the zone of residual stress.

Concurrent with experimental efforts, an analytical approach has been developed and used to predict SCOD for Mode I surface microcracks based on crack geometry. Correlation with independent results for macrocracks and values for microcracks measured in this program are excellent. In addition, an existing computer program has been successfully used to predict SCOD of corner cracks in the absence and presence of an imposed compressive residual stress field.

SECURITY CLASSIFICATION OF THIS PAGE(When Data Entered)

## FOREWORD

The research reported herein was conducted by Southwest Research Institute of San Antonio, Texas, under Contract N00014-78-C-0674. The report summarizes work accomplished during the period August 1979 through July 1980. Dr. Bruce MacDonald was the ONR Program Manager. The work was conducted under the general supervision of Dr. Gerald R. Leverant, SwRI Project Manager, with assistance from Mr. John E. Hack, who acted as Principal Engineer. Special acknowledgement is due to Dr. David L. Davidson, who conducted the in-situ loading experiments in the SwRI SEM and, along with Dr. James Lankford, offered many pertinent suggestions. The assistance of Mr. Harold Saldana in the performance of the X-ray stress measurements and in sample preparation was greatly appreciated.

Accession For	
DTIS	<input checked="checked" type="checkbox"/>
CSA&I	<input type="checkbox"/>
ERIC TAB	<input type="checkbox"/>
Unannounced	<input type="checkbox"/>
Justification	
By	
Distribution/	
Availability Codes	
Dist	Avail and/or
	Special
A	

## TABLE OF CONTENTS

	<u>Page</u>
LIST OF TABLES	v
LIST OF FIGURES	vi
I. INTRODUCTION	1
II. DIRECT OBSERVATION OF SCOD VS. LOAD BEHAVIOR	2
A. Experimental Procedure	2
B. Results and Discussion	9
III. PREDICTION OF SCOD VS. LOAD BEHAVIOR	21
A. Comparison of Predicted and Observed Surface Microcrack Opening	21
B. Prediction of Surface Opening of Corner Cracks Under the Influence of Residual Stress	29
IV. CONCLUSIONS	38
V. REFERENCES	39

## LIST OF TABLES

<u>Table</u>		<u>Page</u>
I	Alloy Compositions	5
II	Uncorrected Surface Values of Residual Stress	10
III	Correlation of Measured and Predicted Microcrack SCOD at Maximum Load	27
IV	Residual Stress Profile in Sample Ti-2	32
V	Scaled Residual Stress Field Used in Calculations for Sample Sample Ti-6	35
VI	Results of BIGIF Calculations on Sample Ti-6 for Applied Stress of 559MPa	37

## LIST OF FIGURES

<u>Figure</u>		<u>Page</u>
1	The Microstructure of the Ti-6Al-4V Material used in This Study	3
2	Microstructure of Quenched and Tempered HY130 (Nital Etch)	4
3	Cantilever Beam Fatigue Specimen	6
4	<u>In-Situ</u> Loading Stage for SEM	7
5	Comparison of SCOD Behavior of Ti-2 and Ti-6 With Compressive Surface Stresses	12
6	Micrographs of SCOD vs. Load in Sample Ti-6 With High Surface Residual Stresses	13
7	Crack Tips in Ti-6Al-4V Samples Under the Influence of High Residual and Applied Loads	16
8	Comparison of SCOD Behavior In Ti-6 Prior to and After Stress Relief	17
9	Comparison of Crack Tip Opening in Sample Ti-6 Prior To and After Stress Relief	18
10	Segment of 200 $\mu$ Crack in an Electropolished Sample	22
11	Microcracks in an Electropolished Sample	22
12	Mode I Cracks in Ground Specimen	24
13	Comparison of Predicted and Measured SCOD Behavior of Microcracks in Ground Specimen	25
14	Fatigue Crack Growth Behavior ( $da/dN$ versus $\Delta K$ ) for Large and Small Cracks in Engineering Alloys	28
15	Crack Profiles in Titanium Samples	30
16	Residual Stress Profile in Sample Ti-6	34

## I. INTRODUCTION

Fatigue cracks in metals generally nucleate at or near a free surface. Since initial growth rates of microcracks are very low ( $\approx 10^{-7}$  in/cycle), fatigue cracks spend a significant portion of their lifetime in the near surface region. Thus the residual stress state at the surface produced by common mechanical and thermal processing can have a marked effect on the fatigue behavior of a material. This report details current results of an ongoing program to quantify the relationship between surface condition and fatigue microcrack growth.

The objective of this program is to quantify the effects of surface residual stresses on surface crack opening displacement (SCOD) behavior. Since COD is directly related to crack growth rate (1,2), this data can be used to correlate surface residual stress state and fatigue behavior. A loading stage which operates in-situ in an SEM is being used to generate SCOD vs. load data for microcracks in Ti-6Al-4V and HY130, a high strength structural steel.

Current results of experimental observations are presented herein which compare SCOD behavior in the absence and presence of a compressive residual stress field. In addition, the initial results of attempts to analytically model SCOD vs. load behavior, based on crack tip stress intensity, are also presented. Surface microcrack opening behavior, experimentally measured during the previous contract year, has been successfully predicted for Mode I opening by this approach. Also, the effects of residual stresses on corner crack opening have been accurately predicted using a boundary integral technique.

## II. DIRECT OBSERVATION OF SCOD VS. LOAD BEHAVIOR

### A. Experimental Procedure

Experiments were continued on Ti-6Al-4V and begun on an HY130 steel alloy. The Ti-6Al-4V material was machined from the rim portion of a pancake forging that was forged at 1241 K in the  $\alpha/\beta$  phase field, annealed for one hour at 1227 K, water quenched and then aged at 977 K for two hours. The resultant microstructure, shown in Figure 1, consisted of primary  $\alpha$  particles embedded in a matrix of transformed  $\beta$  (Widmanstätten  $\alpha$ ) with an  $\alpha$  particle size of approximately  $14\mu$ . Figure 2 shows the structure of the HY-130 steel which was supplied as rolled, quenched and tempered two-inch thick plate. The alloy compositions are summarized in Table I.

A cantilever beam fatigue specimen was used to promote surface crack initiation. Figure 3 shows the tapered gage section which yields a constant stress over the entire gage length. It can be seen from the figure that slots are incorporated in the grip sections to allow for fixturing the specimen into the SEM loading stage after the initiation of cracks in a bending rig.

The SEM loading stage, developed at SwRI (3), is shown in Figure 4. The stage is capable of cyclically loading a sample in tension-tension at loads up to 3800 newtons at frequencies ranging from 0 to 5 Hz while maintaining the area of interest within the viewing screen of the SEM and in focus. Crack behavior can be videotaped and replayed for analysis of crack opening displacement response. In addition, samples can be statically loaded in tension at loads up to 4900 newtons.

Additional samples of the Ti-6Al-4V alloy were machined and shot-peened to an intensity of .011A. The gage sections of two specimens were then

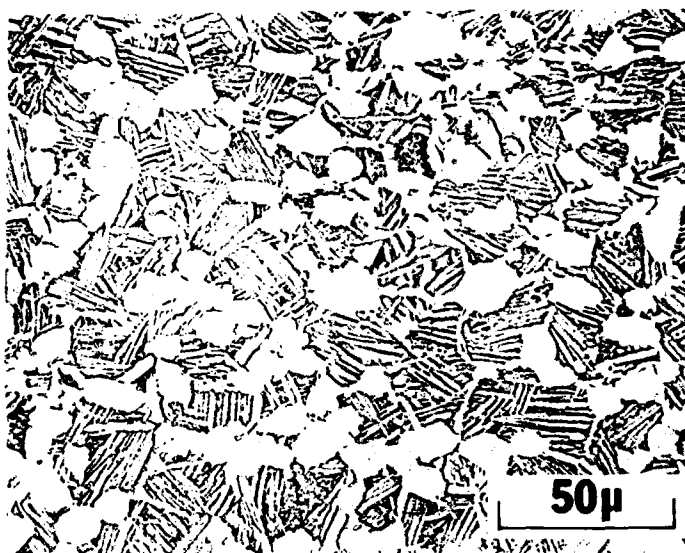


FIGURE 1. THE MICROSTRUCTURE OF THE Ti-6Al-4V MATERIAL USED IN THIS STUDY. The microstructure was developed by forging at 1241°K, annealing for one hour at 1227°K, water quenching and aging for 2 hours at 977°K.

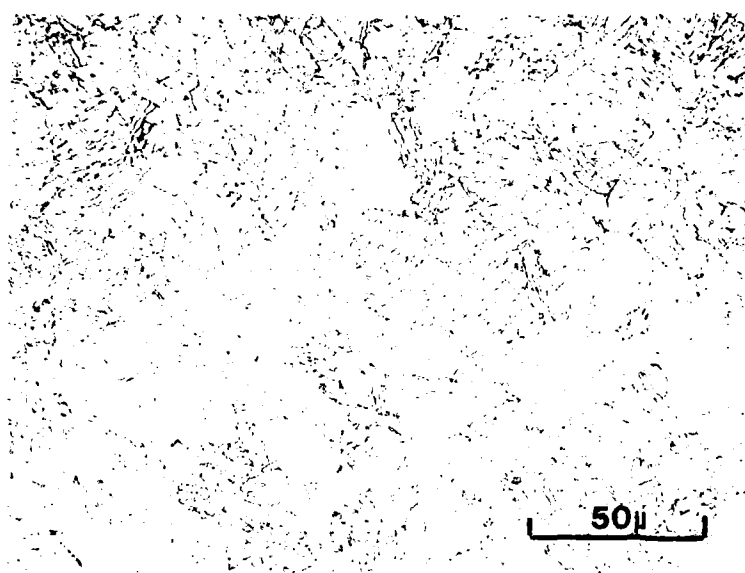


FIGURE 2. MICROSTRUCTURE OF QUENCHED AND TEMPERED HY130  
(NITAL ETCH).

TABLE I  
ALLOY COMPOSITIONS

<u>Material</u>	<u>Element</u>	<u>Wt. Pct.</u>
Ti-6Al-4V*	Al	6.3-6.4
	V	4.3
	Fe	0.10-0.18
	O	0.17-0.18
	N	0.013-0.015
	H	0.005-0.006
HY-130**	C	0.12
	Mn	0.6-0.9
	P	0.01
	S	0.015
	Si	0.20-0.35
	Ni	4.75-5.25
	Cr	0.4-0.7
	Mo	0.3-0.65
	V	0.05-0.1

\* Analyzed Values

\*\* Nominal Values



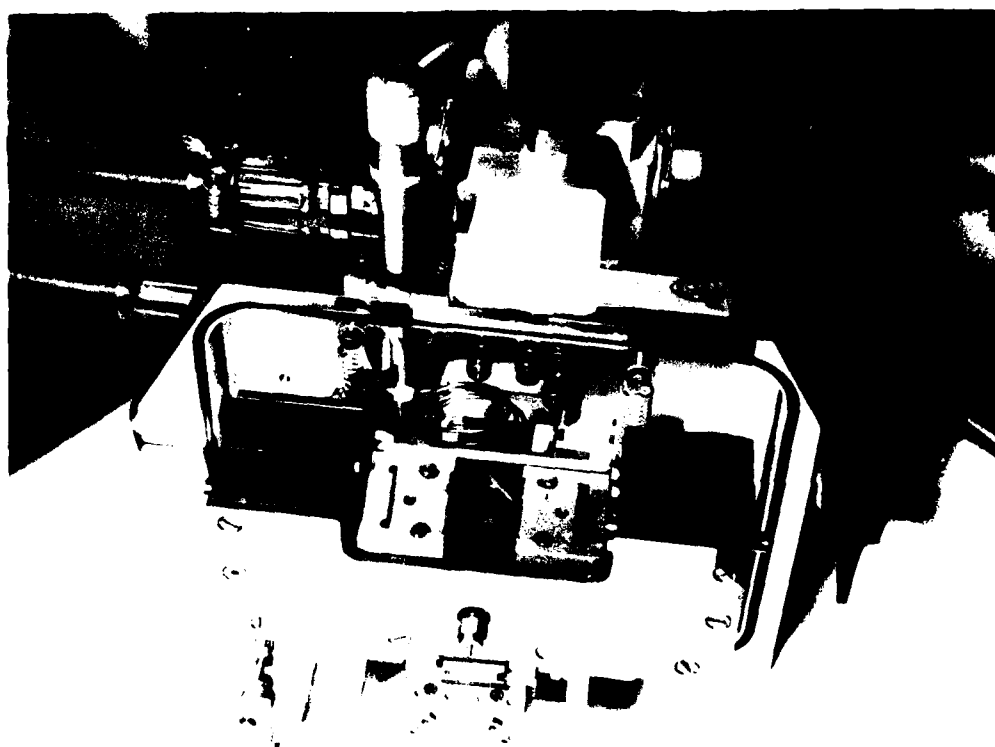


FIGURE 4. IN-SITU LOADING STAGE FOR SEM.  
A fatigue specimen is shown loaded  
in stage.

metallographically polished back to different depths to yield different residual stress levels on the two specimens. The gage sections were electropolished to remove any effects from the mechanical polishing on the residual stress state. An HY-130 sample was machined with its axis parallel to the rolling direction. The sample was then peened to an intensity of .011A and lightly electropolished in the gage section to reveal the microstructure. This was to aid in locating cracks by optical microscopy.

The  $d$  vs  $\sin^2\psi$  X-ray technique (4) was used to measure the residual stress level on all the peened samples. A computer program developed during the first year of this program was used to perform a second degree curve fit to the intensity vs  $2\theta$  data obtained from the X-ray stress measurements. Enough points are used to define the peaks of interest at  $\psi = 0, 30$  and  $45^\circ$ ; then the peak positions and  $d$  spacings are calculated. The slope of  $d$  vs.  $\sin^2\psi$  is obtained and used to calculate the residual stress. The coefficient of correlation for the linear curve fit of the  $d$  vs.  $\sin^2\psi$  is generally in the order of 95-99% indicating a high degree of accuracy in the measurements.

Profiles of residual stress gradients were obtained by measuring the surface stress and then removing a small amount of material by electropolishing. This process was repeated until points were obtained to properly define the gradient. Subsequently, the peak position and residual stress values obtained were used to make corrections due to beam penetration and the relaxation caused by material removal.

A  $0.2^\circ$  receiving slit and a  $3^\circ$  primary beam slit were used for all measurements. The  $3^\circ$  primary beam slit was masked with a 127 $\mu$  thick alpha brass foil to restrict the height of the beam impinging on the sample surface to within

the thickness of the gage section. No Soller slits were used and the measurements for all peaks were performed with the detector at the focus position for each peak. Cu K $\alpha$  radiation with a Ni filter was used in conjunction with the [213] plane of alpha titanium for the stress measurements in Ti-6Al-4V. Cr K $\alpha$  radiation with a vanadium oxide filter was used in conjunction with the [211] plane for the HY-130 steel. The values of  $E/(1+\nu)$  for the titanium and steel alloys were  $8.96 \times 10^4$  and  $1.59 \times 10^5$  MPa, respectively.

The two titanium samples (Ti-2 and Ti-6) were precracked in bending within the strain limits of  $0.45 \pm 0.45\%$  at 1 Hz. All testing was performed at room temperature. Prior to examination of the SCOD behavior, the samples were "shaken down" by several hundred cycles under load control in axial tension in the SEM stage. Load limits used were  $\approx 100$ -600 MPa applied at 3 Hz. Both static and dynamic measurements of the SCOD vs. load behavior were performed on the two titanium specimens. In addition, one of the titanium specimens was stress-relieved after the initial measurements. SCOD vs. load behavior was remeasured on the specimen to gain direct evidence of the effect of residual stress on crack opening. A suitable crack for SCOD measurements has not been obtained on an HY 130 specimen to date. The HY 130 sample described previously is currently being cycled between the strain limits of  $0.15 \pm 0.25\%$ .

#### B. Results and Discussion

The uncorrected surface values of residual stress are presented in Table II. As can be seen from the data, the two titanium specimens differ in surface residual stress by approximately 300 MPa, although both samples have a significant amount of compression at their surfaces.

The crack used for observation in both Ti-2 and Ti-6 ran from one edge

TABLE II

## UNCORRECTED SURFACE VALUES OF RESIDUAL STRESS

<u>Sample</u>	<u>Material</u>	<u>Residual Stress (MPa)</u>
Ti-2	Ti-6Al-4V	-550
Ti-6	Ti-6Al-4V	-850
HY-3	HY-130	-900

towards the center of the specimen. As will be shown later, profiling of the cracks proved them to be corner rather than surface cracks. Micrographs and video tape were taken at the center of the crack and at the crack tip away from the edge on the polished face of the specimen at several loads for each specimen. The measured SCOD values as a function of applied stress are presented for the center of the crack in Figure 5. Any effects of a residual opening have been subtracted out. In both cases the crack remains closed until the stress reaches approximately 300MPa. After that point the SCOD increases approximately linearly with stress. This is illustrated in the sequence of photographs from sample Ti-6 in Figure 6.

Figure 7 shows the crack tips away from the edge in both samples at maximum load. As can be seen from the figures, the tips have only just begun to open, even at loads approaching 560MPa. This indicates that the residual compressive stress present at the surface of the two specimens is strongly influencing the surface CTOD through the entire loading cycle.

Figure 8 presents a comparison of the SCOD vs. load behavior of sample Ti-6 before and after a stress relief heat treatment conducted at 540°C one hour in vacuum. As can be seen from the figure, subsequent to the stress relief treatment, crack opening begins shortly after the application of load. In addition, the opening increases linearly with stress as soon as the crack begins to open.

Above a stress of approximately 350MPa, the SCOD vs. stress curve for the stress-relieved material becomes non-linear. This behavior indicates a plastic yawing open of the crack tip. Such opening is apparent in the sequence of photographs in Figure 9 which contrast the surface CTOD in sample Ti-6 at two loads before and after the stress relief treatment. The photographs show that,

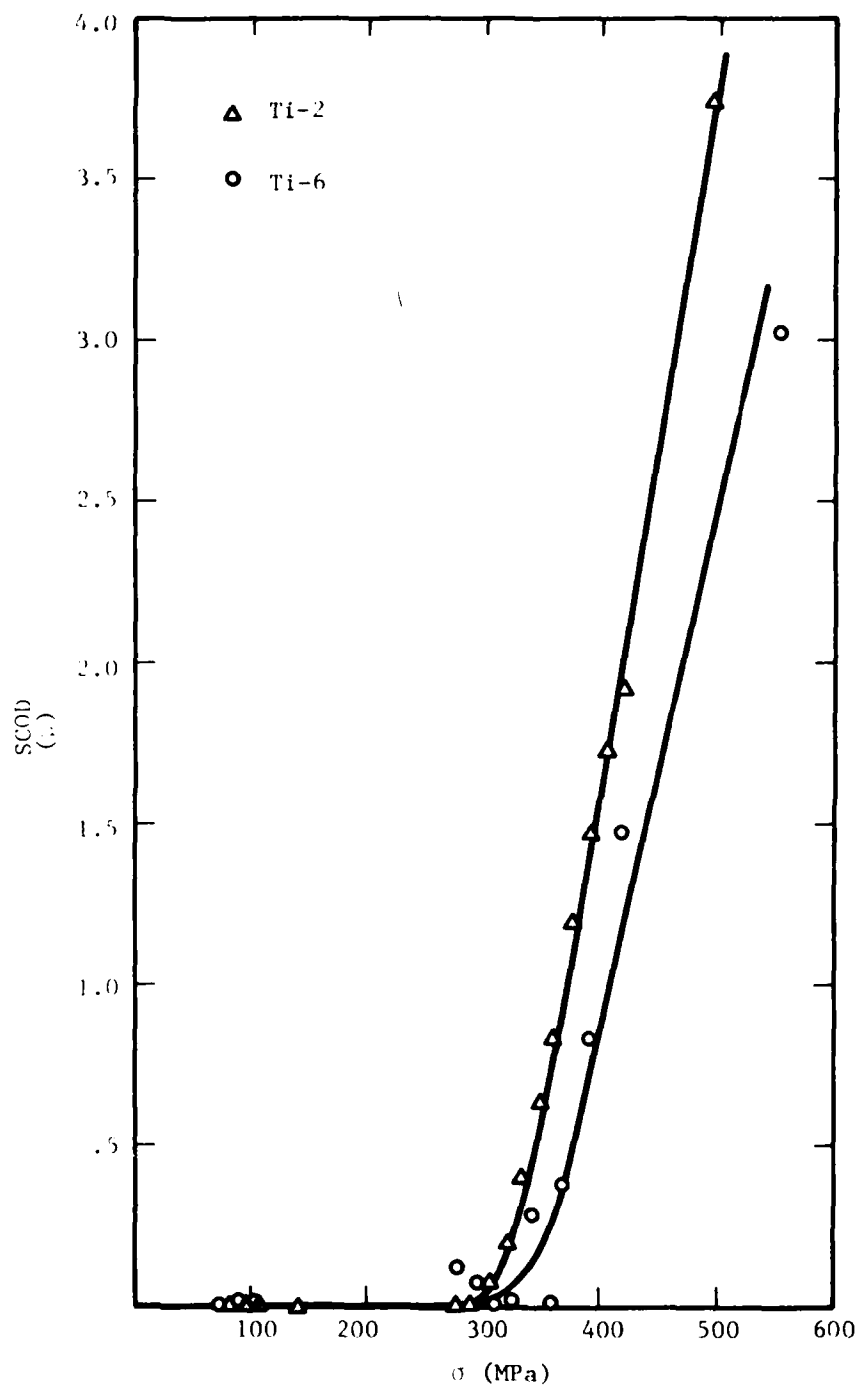
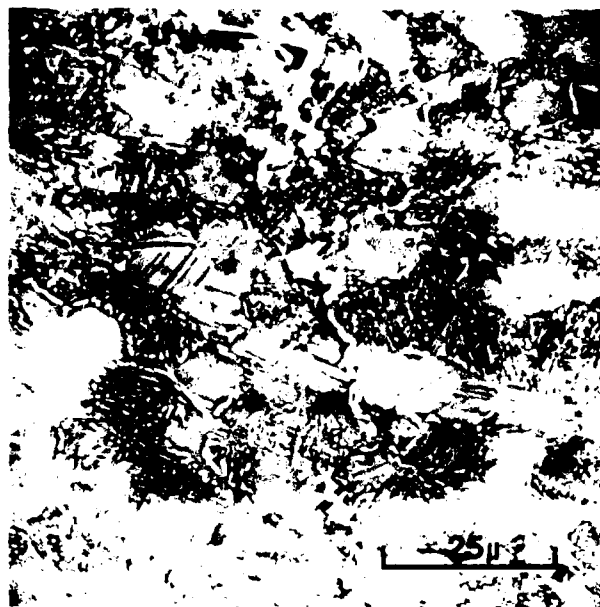
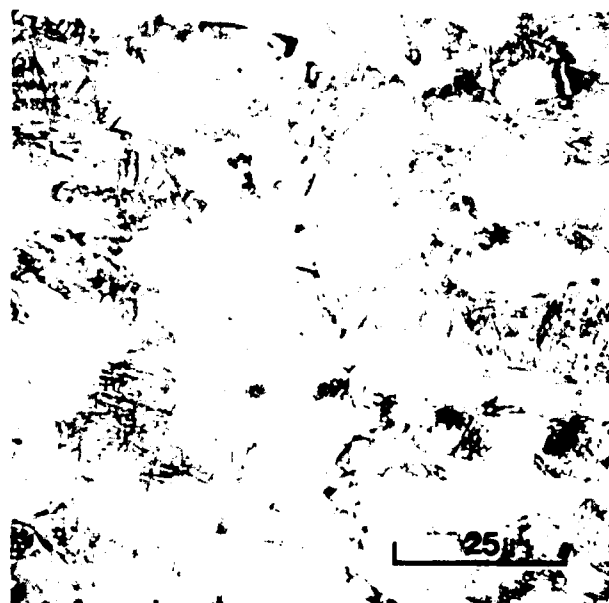


FIGURE 5. COMPARISON OF SCOD BEHAVIOR OF Ti-2 AND Ti-6 WITH COMPRESSIVE SURFACE STRESSES.

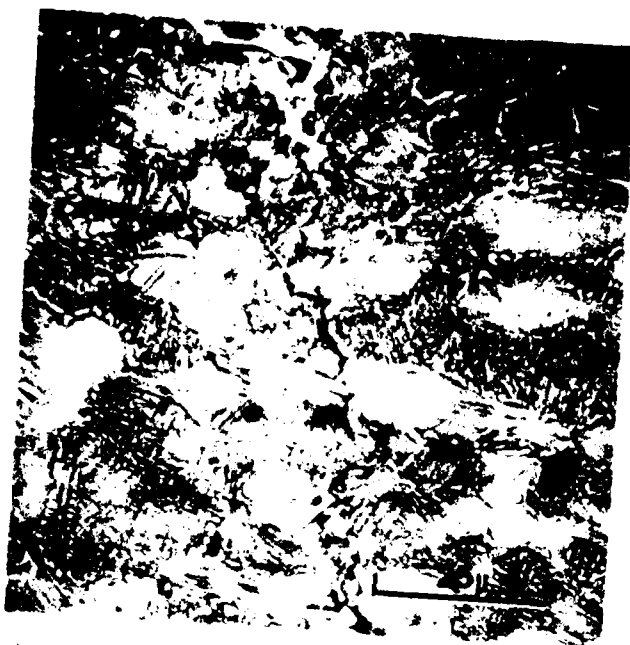


a) 103MPa



b) 274MPa

FIGURE 6. MICROGRAPHS OF SCOD vs. LOAD IN SAMPLE T1-6 WITH HIGH SURFACE RESIDUAL STRESSES.



c) 322MPa



d) 354MPa

FIGURE 6. (continued)

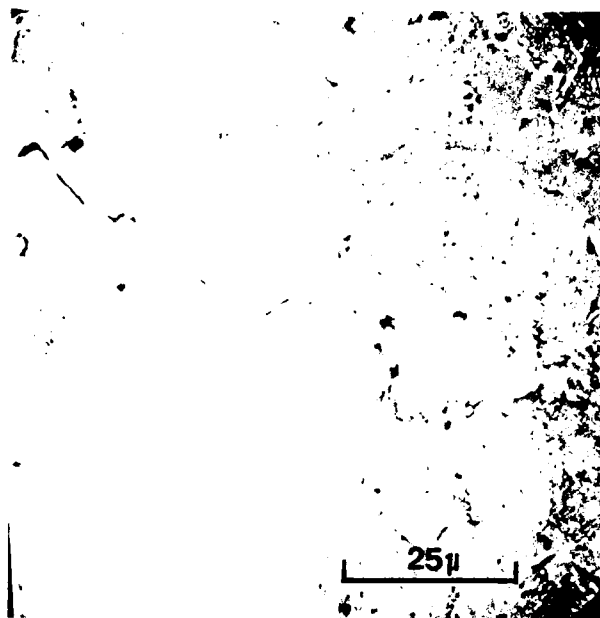


e) 387 MPa

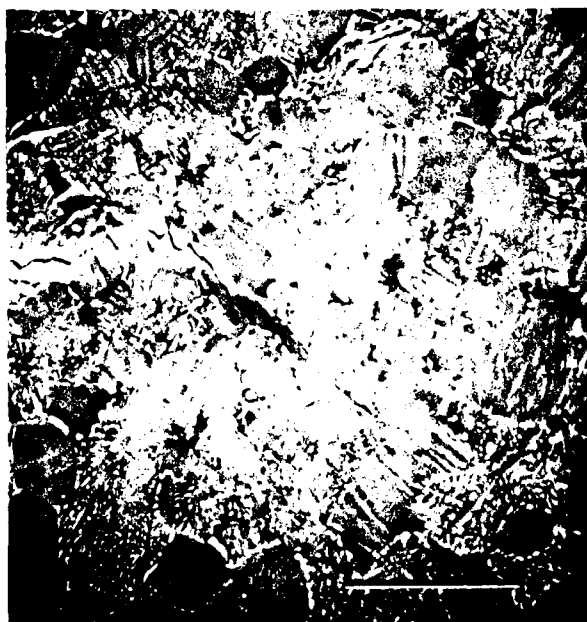


f) 552MPa

FIGURE 6. (continued)



a) Crack tip in Ti-2 @ 494MPa.



b) Crack tip in Ti-6 @ 559MPa.

FIGURE 7. CRACK TIPS IN Ti-6Al-4V SAMPLES UNDER THE INFLUENCE OF HIGH RESIDUAL AND APPLIED LOADS.

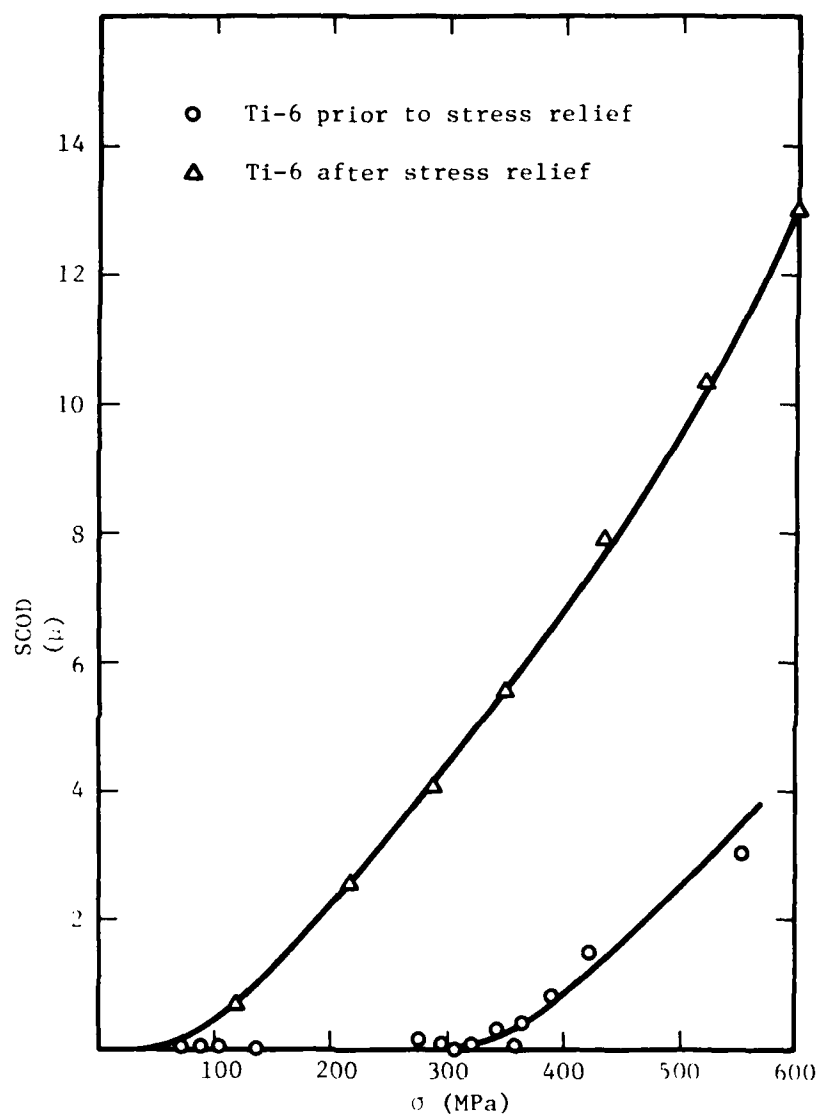
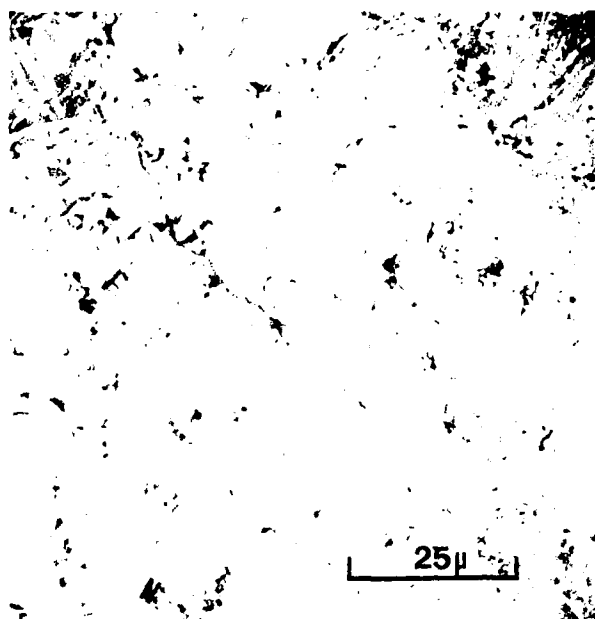
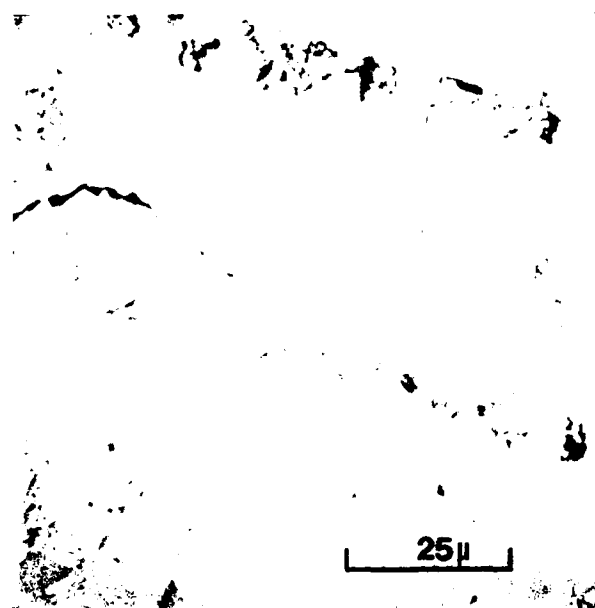


FIGURE 8. COMPARISON OF SCOD BEHAVIOR IN Ti-6 PRIOR TO AND AFTER STRESS RELIEF.



a) Crack tip opening prior to stress relief  
@ 408MPa.

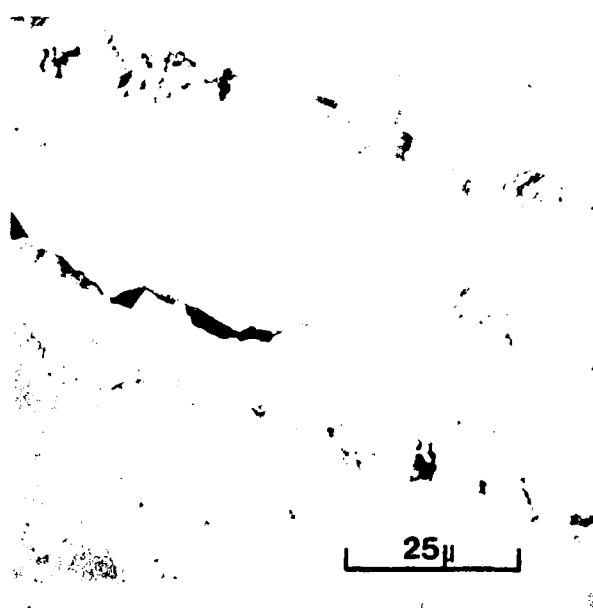


b) Crack tip opening after stress relief  
@ 408MPa.

FIGURE 9. COMPARISON OF CRACK TIP OPENING IN SAMPLE  
Ti-6 PRIOR TO AND AFTER STRESS RELIEF.



c) Crack tip opening prior to stress relief @ 559MPa



d) Crack tip opening after stress relief @ 559MPa

FIGURE 9. (continued)

while the crack tip in Ti-6 in the shot-peened condition remains closed (or nearly so) throughout the entire loading sequence, the crack tip in the stress-relieved condition begins to open with the onset of non-linearity in the SCOD vs. load curve (Figure 8). In addition, while no growth occurred during the experiments performed on the two samples in the shot-peened condition, Figure 9 shows that the crack in Ti-6 did propagate across several grains ( $\approx 40\mu$ ) during the course of the experiment after the stress relief treatment. This crack growth can actually be observed in the video tape.

### III. PREDICTION OF SCOD VS. LOAD BEHAVIOR

#### A. Comparison of Predicted and Observed Surface Microcrack Opening

As reported at the end of the previous contract year (5), an analytical approach to the prediction of SCOD behavior of surface microcracks was developed. The approach was based on the use of closed form expressions for the crack tip stress intensity of a surface crack, as given by Gray (6). The approach was successfully applied to the prediction of SCOD of a 5000 $\mu$  long surface microcrack from independent work (7). Although general predictions on microcrack behavior were obtained at that time, no application to the concurrently generated microcrack data was possible due to a lack of information on crack geometry. This information was obtained during the current contract year and was used to test the applicability of the approach.

Figures 10-12 show the microcracks used in experiments during the previous contract year. It will be recalled that very little or no surface residual stresses were present in any of these specimens. Crack geometries were obtained by placing several microhardness indents of known geometry near the cracks and then metallographically polishing the sample surfaces until the cracks disappeared. Crack depths were obtained by following changes in the length of the Knoop indents, which can be related to their depth by a factor of one-thirtieth.

Figure 13 shows a comparison of measured vs. predicted behavior for two microcracks in a surface ground parallel to the stress axis of the specimen (Figure 12). As can be seen from Figure 13, the experimental and predicted results match up very well for these cases. Figure 12 shows that the cracks are quite straight and perpendicular to the stress axis. Since the analytical

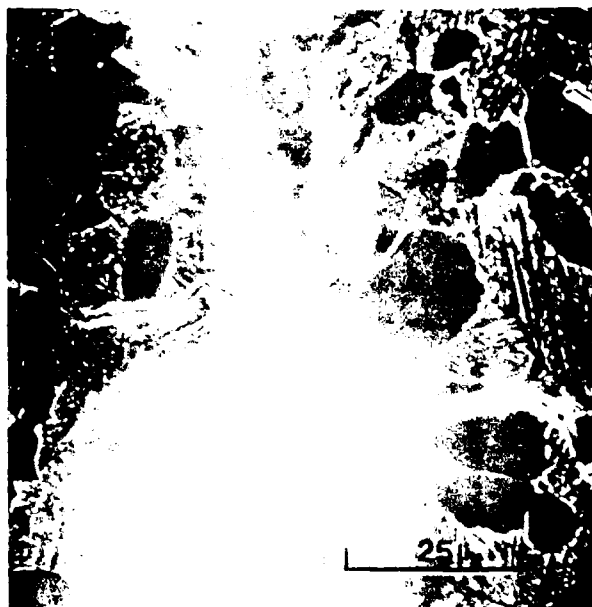


FIGURE 10. SEGMENTED SURFACE IN ELECTROPOLISHED SAMPLE.

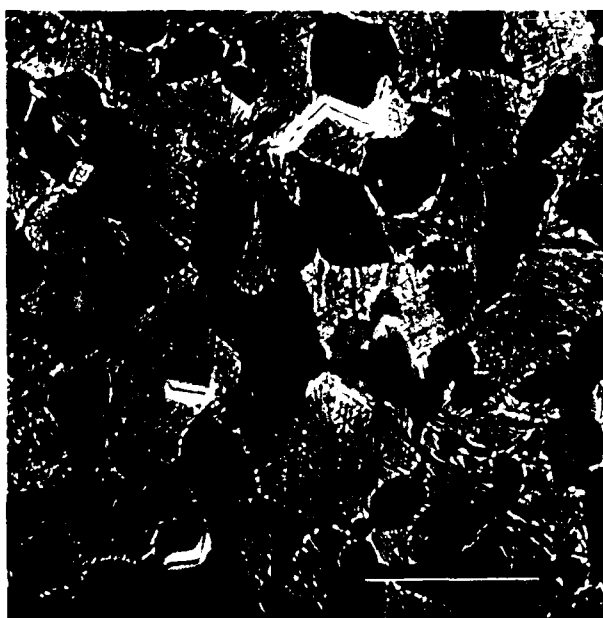


(a) 100x

FIGURE 11. SURFACE IN ELECTROPOLISHED SAMPLE.



b) 83H crack



c) 18 and 7: crack

FIGURE 11. (continued)

a) 50 $\mu$  crackb) 32 $\mu$  crack

FIGURE 12. MODE I CRACKS IN GROUND SPECIMEN

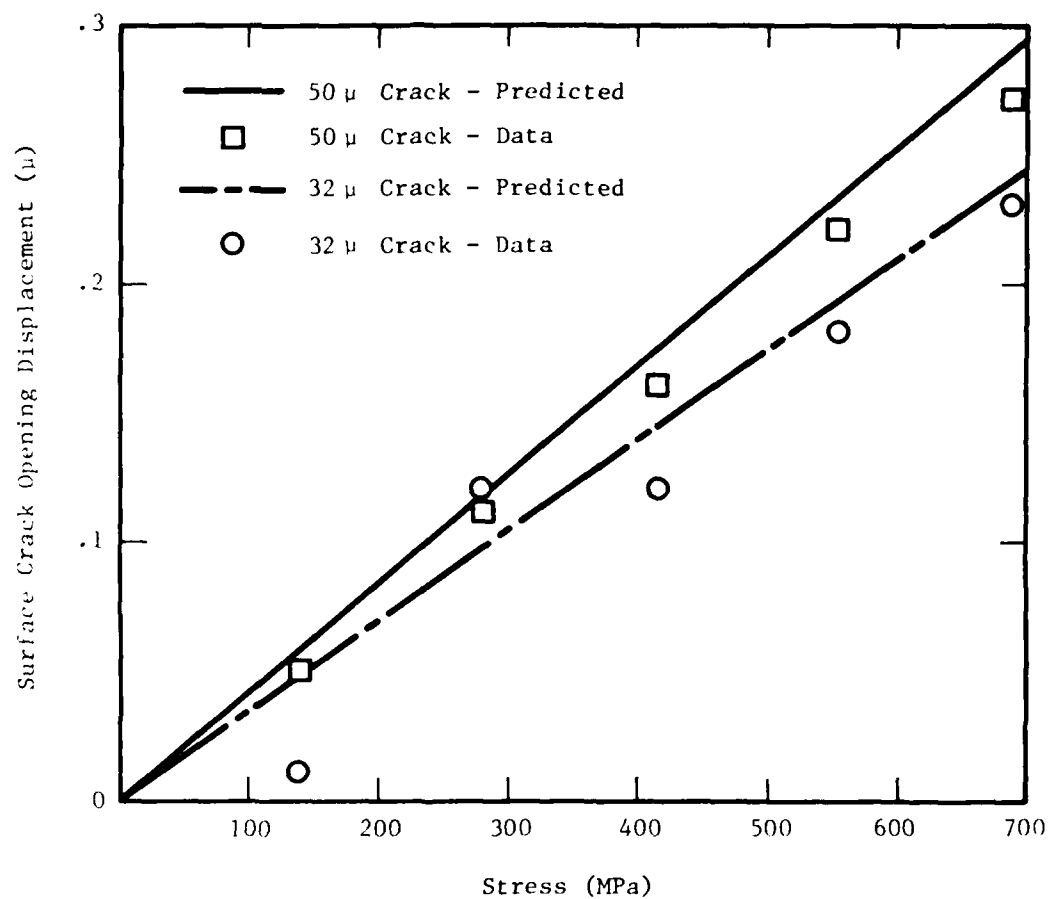


FIGURE 13. COMPARISON OF PREDICTED AND MEASURED SCOD BEHAVIOR OF MICROCRACKS IN GROUND SPECIMEN.

approach was developed on the basis of Mode I loading, the good agreement between theory and experiment is very encouraging.

Table III shows a comparison of data for all the microcracks observed during the previous contract year that have been fully analyzed to date. The experimental and predicted SCOD values given represent those taken at 700MPa, which was the maximum load possible before gross plasticity occurred at the tips of the cracks. The data for the ground specimen are the same as in Figure 13. However, the agreement is not as good for the crystallographic cracks observed in electropolished specimens.

In the case of the 200 $\mu$  crystallographic surface crack in an electropolished sample (Figure 10), the predicted value ran twice that observed in the SEM. This is probably due to the fact that the mixed mode nature of the crack would tend to reduce the opening normal to the stress axis from the value obtained for a pure Mode I case. Predicted openings for the 63, 53, 18 and 7 $\mu$  crystallographic cracks in the second electropolished sample (Figure 11) were much lower than those actually measured. These cracks are on the order of or smaller than the primary  $\alpha$  grain size (14 $\mu$ ) in at least one dimension. Thus, the Mode I linear elastic fracture mechanics approach used for the predictions would not be expected to hold. Data are available on very small cracks in several engineering alloys which show that cracks on the order of the grain size deviate from crack growth behavior for macrocracks. Figure 14 shows that, in the case of a mild steel and an aluminum alloy, microcracks grow considerably faster than large macrocracks, while microcracks grow more slowly in a Ni base alloy and a high strength steel.

TABLE III  
CORRELATION OF MEASURED AND PREDICTED MICROCRACK  
SCOD AT MAXIMUM LOAD

Surface Condition	Type of Cracking	Crack Length ( $\mu$ )	a/c	Measured SCOD @ 690 MPa ( $\mu$ )	Predicted SCOD @ 690 MPa ( $\mu$ )
Electropolished	Crystallographic	200	.25	.40	.77
		63	.35	.49	.31
		53	.36	.37	.27
Electropolished	Crystallographic	18	.39	.31	.10
		7	1.0	.30	.07
Ground    to Stress Axis	Mode I	50	.45	.27	.29
		32	.70	.20	.24

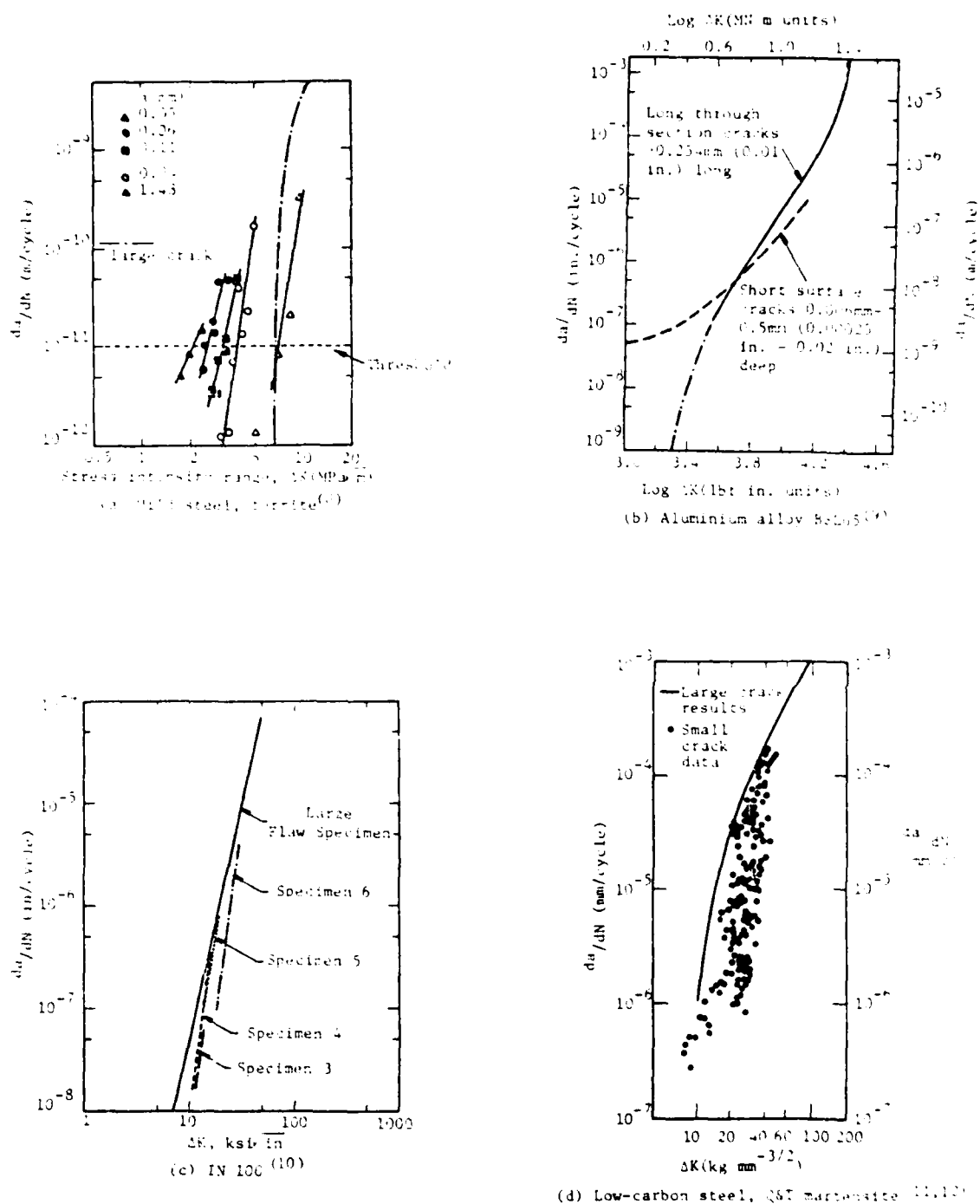


FIGURE 14. FATIGUE CRACK GROWTH BEHAVIOR ( $da/dN$  versus  $\Delta K$ ) FOR LARGE AND SMALL CRACKS IN ENGINEERING ALLOYS.

B. Prediction of Surface Opening of Corner Cracks Under the Influence of Residual Stress

Since the cracks in Ti-2 and Ti-6 were much larger than those previously studied and they extended to the specimen edge, small portions containing the cracks were cut from the specimens and profiled by polishing in from the edge. The results of the profiling are presented in Figure 15. As can be seen from the figures, not only are the cracks in Ti-2 and Ti-6 much larger than those previously discussed, they are also corner rather than surface cracks. The cracks extend almost one-third of the way across the gage width of the specimens and are over one-half the thickness deep. The large size of the two cracks precluded any difficulties with the application of linear elastic fracture mechanics to their analysis despite their crystallographic nature. As was the case for the 5000 $\mu$  long surface crack discussed earlier, crystallographic effects will tend to average out over the length of the crack if it is much larger than the grain size. Since the cracks could not be properly treated as surface cracks and, if they were treated as such, their  $a/c$  ratio would be greater than one, these cracks were not amenable to treatment by the previously described analytical approach.

To overcome this problem, a computer program was used (13) that is capable of calculating stress intensities for several crack geometries, including the corner crack. Another reason for the selection of this program is the ability to incorporate a residual stress gradient in the calculations. The program is called BIGIF (Boundary Integral Generated Influence Functions).

Figure 16 shows the residual stress profile measured in sample Ti-2 by the  $d$  vs.  $\sin^2 \psi$  X-ray technique described earlier. Table IV gives the values of stress after they have been corrected for beam penetration and layer removal.

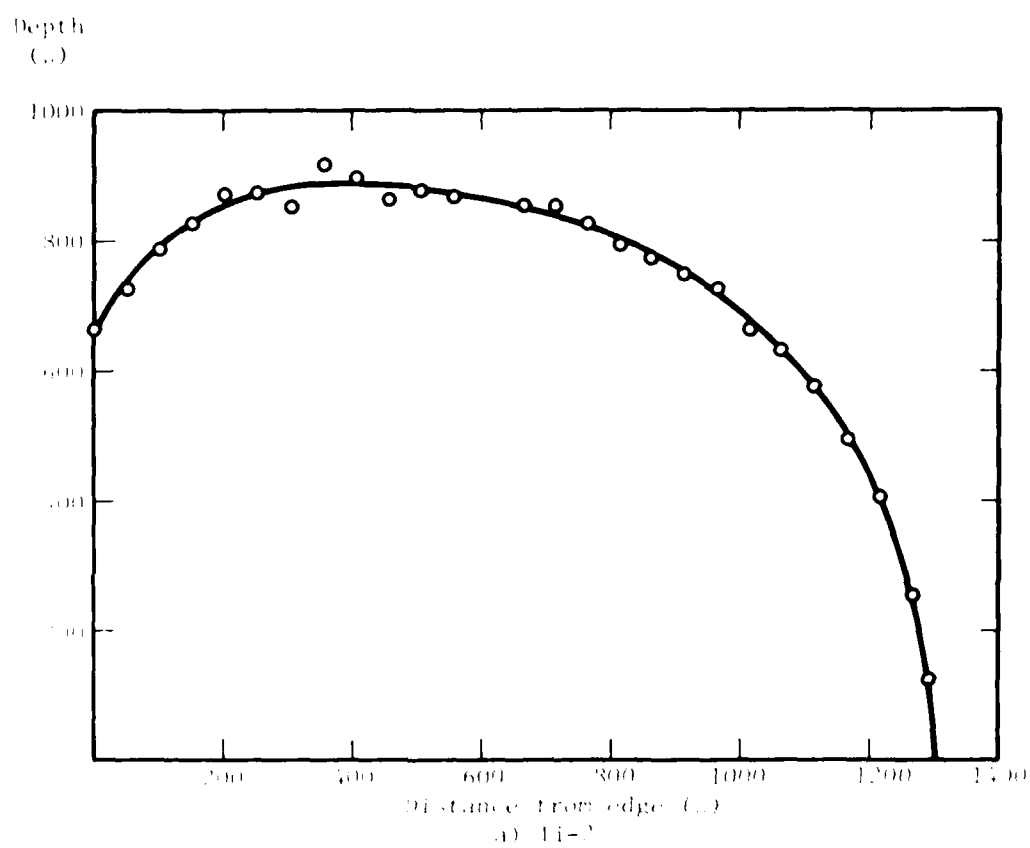


FIGURE 15. CRACK PROFILES IN TITANIUM SAMPLES

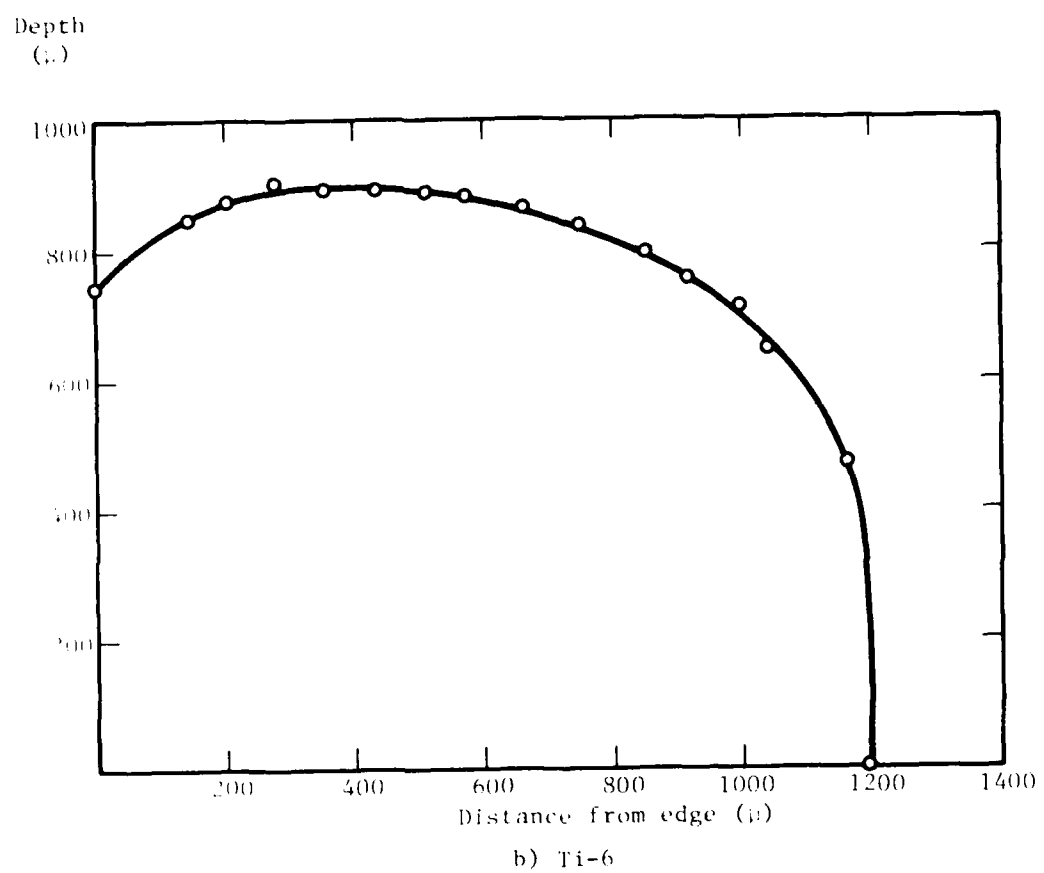


FIGURE 15. (continued)

TABLE IV

## RESIDUAL STRESS PROFILE IN SAMPLE Ti-2

<u>Depth (<math>\mu</math>)</u>	<u>Residual Stress (as measured) (MPa)</u>	<u>Residual Stress (corrected for beam penetration) (MPa)</u>	<u>Residual Stress (corrected for beam penetration and layer removal) (MPa)</u>
0.0	-551	-555	-555
10.2	-599	-600	-563
20.3	-600	-600	-550
27.9	-602	-600	-540
38.1	-584	-577	-516
45.7	-532	-533	-482
73.7	-510	-489	-420
101.6	-360	-355.5	-302
167.6	-239	-245	-124

As can be seen from the data, the residual stress initially decreases to a maximum compressive stress and then rises sharply as the depth increases. It is significant to note that an extrapolation of the curve in Figure 16 to zero residual stress will occur at only 212 $\mu$  in depth. This means that the residual stress field had a significant effect on surface crack opening even when the crack extended over four times as deep as the zone of significant residual compression. Although the exact profile for Ti-6 is only presently being determined, the depth of residual stress should only be dependent on peening intensity. Since the two specimens were initially peened at the same intensity, a similar result is expected in Ti-6.

Since the residual stress field in Ti-2 is complicated by the fact that the edge stress field is much more intense than the polished face, initial calculations were performed for Ti-6. Only a very slight amount of material was removed from the surface of this specimen ( $\approx 50\mu$ ). The residual stress field was assumed by scaling the profile of Ti-2 with respect to the surface stress values for the two specimens. For purposes of the calculation, the residual stress was chosen to go to zero at an appropriate depth (approximately 250 $\mu$  as obtained from the scaling factor) and remain at that level until the back surface residual compression was encountered. This is a good assumption since the depth of significant residual compression is small in comparison to the width and thickness of the specimen. The estimated values, given in Table V, were assumed to be valid around the perimeter of the gage section. The calculations will be repeated when the actual residual stress field is obtained.

Results of the predicted values of SCOD in Ti-6 both prior to and after stress relief using BIGIF generated stress intensities are presented in

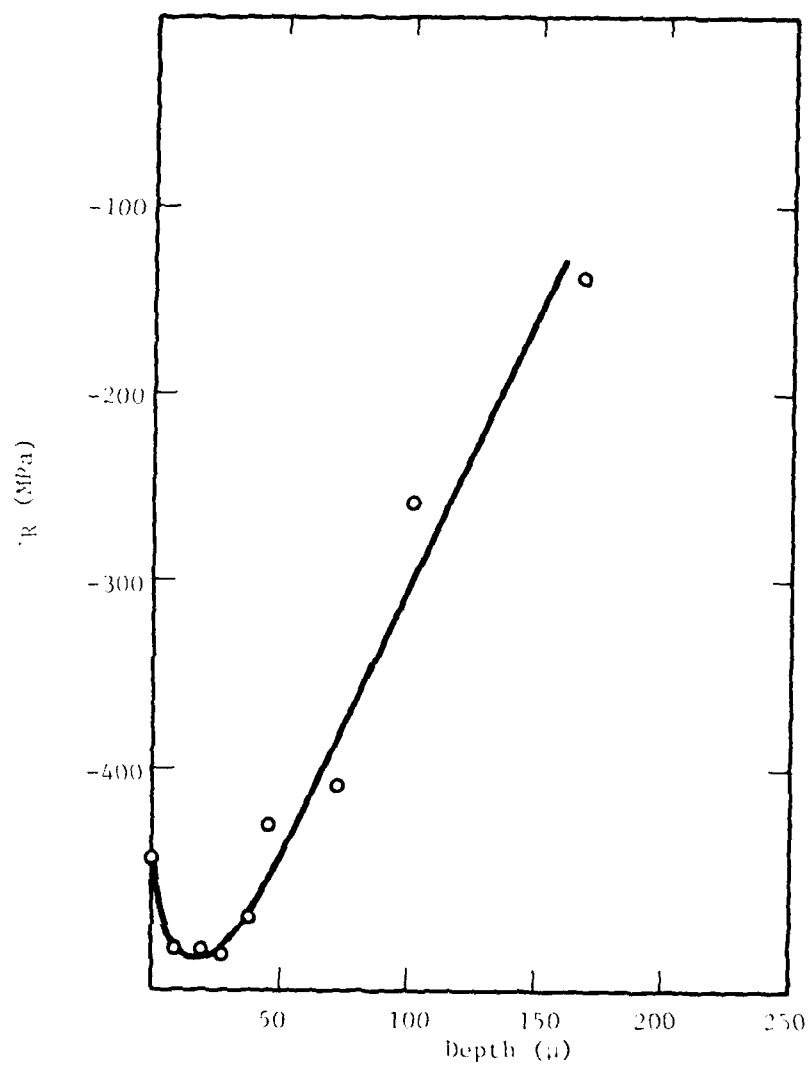


FIGURE 16. UNCORRECTED RESIDUAL STRESS PROFILE IN SAMPLE Ti-6.

TABLE V

SCALED RESIDUAL STRESS FIELD USED IN CALCULATIONS FOR  
SAMPLE Ti-6

<u>Depth (<math>\mu</math>)</u>	<u>Residual Stress (MPa)</u>
0.0	-862
190.5	-945
254	0

Table VI with the measured openings for comparison. Use of the calculated surface crack tip stress intensities, also given in the table, yield values of opening which agree very well with those observed in the sample both prior to and after the removal of the compressive residual stress field. This result emphasizes the strong influence that the surface stresses have on surface crack opening, and thus crack growth, behavior. Even after the majority of the crack has moved out of the residual stress field, the surface opening is still reduced substantially by the compressive surface stress state and consequently surface crack growth is reduced. This observation has strong implications for retirement-for-cause and leak-before-break approaches to component design and removal from service.

TABLE VI

RESULTS OF BIGIF CALCULATIONS ON SAMPLE T1-6  
FOR APPLIED STRESS OF 559MPa

<u>Condition</u>	<u>K<sub>sur</sub> (MPa)</u>	<u>SCOD*<sub>(psur)</sub> (μ)</u>	<u>SCOD**<sub>(meas)</sub> (μ)</u>
Prior to Stress Relief	4.7	2.85	3.1
After Stress Relief	21.5	12.97	11.34

\* Predicted from surface crack tip stress intensity ( $SCOD = 4\sqrt{\frac{2r}{\pi}} (1-\nu^2) \frac{K}{E}$ )

\*\* Measured

## IV. CONCLUSIONS

1. Surface residual stresses can significantly influence crack opening, and thus crack growth, even after the crack has grown well out of the zone of residual stress.
2. The analytical approach developed in this program can be used to predict the opening of Mode I surface microcracks with a good deal of accuracy.
3. The influence of a surface residual stress field on surface crack tip stress intensities and crack opening behavior can be accurately predicted with an existing computer program (BIGIF).

## V. REFERENCES

1. A. J. McEvily and T. L. Johnston, Int. J. Frac. Mech., vol. 3, 1967 p. 45.
2. G. G. Garrett and J. F. Knott, Met. Trans., vol. 74, 1976, p. 884.
3. D. L. Davidson and A. Nagy, J. Phys. E (Sci. Inst.), vol. 11, 1978 p. 207.
4. E. Macherauch, Exp. Mech., vol. 6, 1966, p. 140.
5. J. E. Hack and G. R. Leverant, Fatigue Microcrack Behavior Under the Influence of Surface Residual Stresses, Interim Report, Contract N00014-78-C-0674, October 1, 1979 (also Int. J. Frac., vol. 16, 1980, p. R15)
6. T.G.F. Gray, Int. J. Frac., vol. 13, 1977, p. 65.
7. J. E. Collipriest, Jr., The Surface Crack: Physical Problems and Computational Solutions, ASME, New York, 1972, p. 43.
8. Y. Nakai and K. Tamaka, Proc. Jap. Cong. Mat. Res., 1980, in press.
9. S. Pearson, Eng. Frac. Mech., vol. 7, 1975, p. 235.
10. J. Lankford, T. S. Cook and G. P. Sheldon, Int. Journ. Frac., in press.
11. T. Yokobori, M. Tanada, H. Hayokawa, T. Yoshimura and S. Sasahira, Reports of the Research Institute for Strength and Fracture of Materials, vol. 3, 1967, p. 39.
12. T. Yokobori, H. Kuribayashi, M. Kawagishi and N. Takeuchi, Reports of the Research Institute for Strength and Fracture of Materials, vol. 7, 1971, p. 1.
13. P. M. Besuner, D. C. Peters and R. C. Cipolla, BIGIF Fracture Mechanics Code for Structures, Key Phase Report, NP-838 Research Project 700-1, EPRI, July 1978.